Title

Upper-ocean-to-atmosphere radiocarbon offsets imply fast deglacial carbon dioxide release

Journal

Nature, 466(7310)

ISSN

0028-0836

Authors

Rose, Kathryn A
Sikes, Elisabeth L
Guilderson, Thomas P
et al.

Publication Date

2010-08-01

DOI

10.1038/nature09288

Peer reviewed

LETTERS

Upper-ocean-to-atmosphere radiocarbon offsets imply fast deglacial carbon dioxide release

Kathryn A. Rose[1]†*, Elisabeth L. Sikes[2]*, Thomas P. Guilderson[3,4], Phil Shane[5], Tessa M. Hill[1], Rainer Zahn[6] & Howard J. Spero[1]

Radiocarbon in the atmosphere is regulated largely by ocean circulation, which controls the sequestration of carbon dioxide (CO_2) in the deep sea through atmosphere–ocean carbon exchange. During the last glaciation, lower atmospheric CO_2 levels were accompanied by increased atmospheric radiocarbon concentrations that have been attributed to greater storage of CO_2 in a poorly ventilated abyssal ocean[1,2]. The end of the ice age was marked by a rapid increase in atmospheric CO_2 concentrations[2] that coincided with reduced $^{14}C/^{12}C$ ratios ($\Delta^{14}C$) in the atmosphere[3], suggesting the release of very 'old' (^{14}C-depleted) CO_2 from the deep ocean to the atmosphere[3]. Here we present radiocarbon records of surface and intermediate-depth waters from two sediment cores in the southwest Pacific and Southern oceans. We find a steady 170 per mil decrease in $\Delta^{14}C$ that precedes and roughly equals in magnitude the decrease in the atmospheric radiocarbon signal during the early stages of the glacial–interglacial climatic transition. The atmospheric decrease in the radiocarbon signal coincides with regionally intensified upwelling and marine biological productivity[4], suggesting that CO_2 released by means of deep water upwelling in the Southern Ocean lost most of its original depleted-^{14}C imprint as a result of exchange and isotopic equilibration with the atmosphere. Our data imply that the deglacial ^{14}C depletion previously identified in the eastern tropical North Pacific[5] must have involved contributions from sources other than the previously suggested carbon release by way of a deep Southern Ocean pathway[5], and may reflect the expanded influence of the ^{14}C-depleted North Pacific carbon reservoir across this interval. Accordingly, shallow water masses advecting north across the South Pacific in the early deglaciation had little or no residual ^{14}C-depleted signals owing to degassing of CO_2 and biological uptake in the Southern Ocean.

Observations in the glacial atmosphere of higher radiocarbon activity ($\Delta^{14}C$) accompanied by lower CO_2 concentrations, relative to modern values[2,6,7], are believed to have been caused primarily by climate-induced changes in the ocean's thermohaline circulation isolating abyssal ocean carbon from the atmosphere[1]. Although independent estimates of ^{14}C production indicate that changes in thermohaline circulation cannot fully account for atmospheric $\Delta^{14}C$ changes since the last ice age[6], considerable evidence suggests that CO_2 with a ^{14}C content significantly lower than it is today was sequestered in the deep glacial ocean below a depth of 2.5 km (refs 8–11). Whereas the full extent of the deep carbon reservoir remains to be constrained[12], it seems that a significant portion of this glacially sequestered CO_2 was reintroduced into the atmosphere by means of ocean outgassing during the last glacial–interglacial transition[3]. This ^{14}C-depleted carbon contributed to atmospheric CO_2 increase[2] while reducing the atmospheric radiocarbon signal by ~20% (ref. 7), leaving a strong imprint on the $\Delta^{14}C$ distribution in the ocean[5,8]. Because deep water masses outcrop in the Southern Ocean, surface processes there probably regulated carbon injection into the atmosphere and CO_2 partitioning among the several ocean reservoirs[1]. Correlations among Antarctic temperature records[13], deglacial atmosphere CO_2 increase[2], changes in Southern Ocean upwelling[4] and model results[14] support this explanation. However, there is still no direct verification of the pathways taken by ^{14}C-depleted CO_2 from the deep ocean to the atmosphere.

Here we present early deglacial surface and intermediate-depth $\Delta^{14}C$ profiles that were reconstructed using radiocarbon activities from coexisting planktonic and benthic foraminifera in two sediment cores in the sub-Antarctic and subtropical South Pacific near New Zealand. The region and shallow water depths of both core sites are ideal for assessing deglacial ^{14}C changes in sub-Antarctic mode water (SAMW; core RR0503-JPC64) and Antarctic intermediate water (AAIW; core MD97-2120) that are derived from the entrainment of abyssal water masses into the upper-ocean thermocline by wind-driven upwelling in the Southern Ocean[15] (Fig. 1). Subtropical mode water (STMW) has components of SAMW entrained from equatorial undercurrent waters or can be partially sourced through the Tasman Sea[15,16].

The baseline age model for core MD97-2120 on the south Chatham Rise (east of New Zealand) is anchored with ^{14}C dating[17] and fine-tuned between 13 and 19 kyr BP by correlating the stable oxygen isotope ($\delta^{18}O$) record of its planktonic foraminifera with the $\delta^{18}O$ record of the European Project for Ice Coring in Antarctica (EPICA) Dronning Maud Land (EDML) ice core[13] (Fig. 2a and Supplementary Fig. 1). This age model allows the use of ^{14}C as a tracer that is not biased by using it as a stratigraphic tool. The age model for core RR0503-JPC64 in the Bay of Plenty (north of New Zealand) was developed by combining ^{14}C-derived calendar-age tie points from the planktonic foraminifera *Globorotalia inflata* with tephra chronology from the core[18] tied to established New Zealand chronologies[19] and the $\delta^{18}O$ record of the EDML ice core[13]. Tephra stratigraphy suggests continuous sedimentation throughout the early deglaciation, before ~13,700 calendar years BP (the Waiohau tephra). However, above this tephra, there seems to be a 4.1-kyr hiatus. For both cores, we used the CALIB v5.0.1 program and MARINE04 database to convert the radiocarbon data to calendar ages. (See Supplementary Information for stratigraphic and methodological details.)

[1]Department of Geology, University of California, Davis, California 95616, USA. [2]Institute of Marine and Coastal Sciences, Rutgers University, 71 Dudley Road, New Brunswick, New Jersey 08901, USA. [3]Lawrence Livermore National Laboratory, Livermore, California 94550, USA. [4]Institute of Marine Sciences, University of California, Santa Cruz, California 95064, USA. [5]School of Environment, University of Auckland, Auckland 1142, New Zealand. [6]Institució Catalana de Recerca i Estudis Avançats, ICREA, Universitat Autònoma de Barcelona, Institut de Ciència i Tecnologia Ambientals, Departmento de Geologia, 08193 Bellaterra, Spain. †Present address: Department of Geology and Geophysics, Woods Hole Oceanographic Institution, Woods Hole, Massachusetts 02540, USA.
*These authors contributed equally to this work.

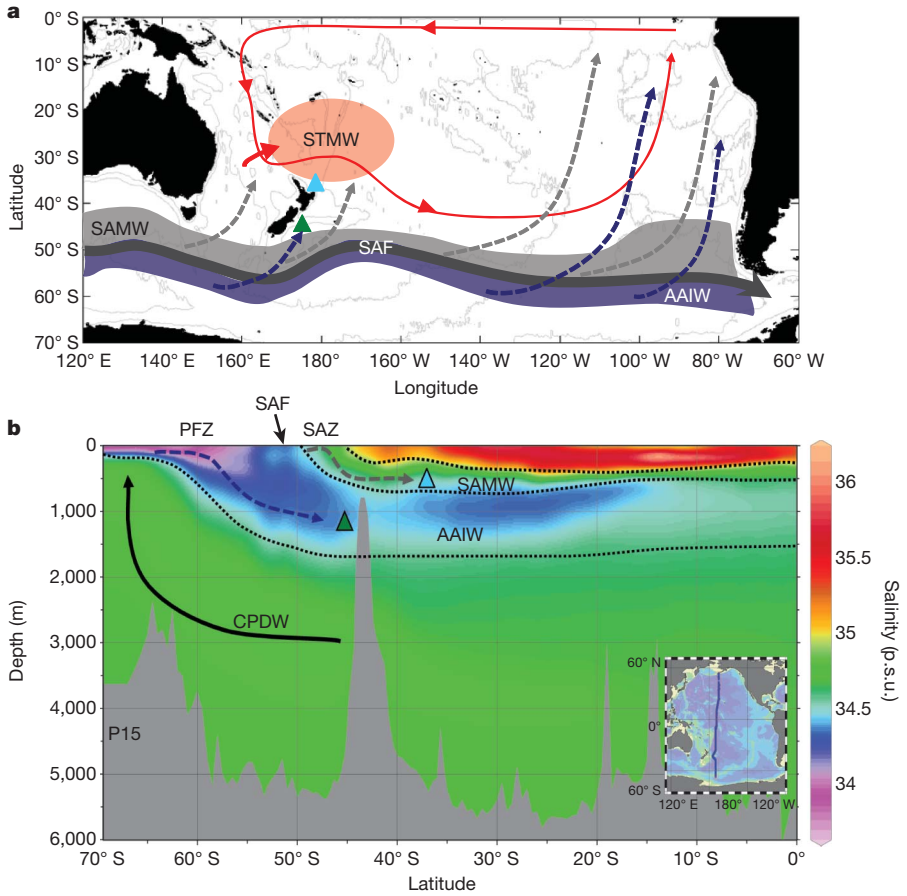

Figure 1 | Ocean circulation in the South Pacific and Southern Ocean and ambient water-mass patterns at the location of the sediment cores used in this study. a, Schematic presentation of major currents. The bold solid line marks the approximate location of the sub-Antarctic front (SAF), which separates cold and fresher polar surface waters, to the south, from the warmer and saltier surface waters in the sub-Antarctic zone (SAZ), to the north. SAMW forms in the SAZ (grey shaded area) and becomes entrained in the South Pacific subtropical gyre circulation (solid red line). At the equator, its chemical signal can be identified in STMW (~100–300-m water depth) in the western basin. Denser AAIW (~800–1,400-m water depth) forms south of the SAF, in the polar frontal zone (PFZ, blue shaded area), and flows northwards below SAMW. The triangles mark the core sites used in this study: RR0503-JPC64 (37° 25.34′ S, 177° 00.41′ E; 651 m; turquoise triangle) and MD97-2120 (43° 32.06′ S, 174° 55.85′ E; 1,210 m; green triangle). **b**, Wind-driven upwelling in the Southern Ocean causes shallow, mid-depth and deep-water masses to shoal. Cores RR0503-JPC64 and MD97-2120 are proximal to the formation zones of SAMW and AAIW and are positioned within the flow paths of both water masses as they are advected to the north and ventilate the South Pacific thermocline. In the Pacific, circumpolar deep water (CPDW) resides below SAMW and AAIW, providing a source for upwelled waters in the Southern Ocean. In the modern ocean, CPDW carries a strong contribution from North Atlantic Deep Water (NADW) flowing out of the Atlantic Ocean at abyssal depths. Inset, ship's track/sampling transect for the salinity vertical profile shown in the main panel. p.s.u., practical salinity units.

To assess partitioning of ^{14}C among the atmosphere, subsurface and surface water masses, we compared age-corrected water-mass $\Delta^{14}C$ values based on foraminifera with contemporary atmosphere values, IntCal04[20] and Cariaco[7], on the Hulu cave timescale[5] (Fig. 2). The two atmospheric ^{14}C levels are offset through the early deglaciation (Fig. 3a), which can be attributed to IntCal04 pre-dating Cariaco on the Hulu cave timescale[6]. Owing to higher sample density, we consider the Cariaco–Hulu record[7] better suited for comparison with our marine radiocarbon records. The planktonic species *G. inflata* in core RR0503-JPC64 is well suited to tracing STMW because it inhabits the upper thermocline, at the depth of STMW. SAMW is advected rapidly, on the order of decades[21], from the sub-Antarctic zone to the tropics, where its $\Delta^{14}C$ signal is entrained upwards into STMW and recorded by *G. inflata*[1] (Fig. 1).

During the early deglaciation, from 18 to 15.8 kyr BP, the benthic and planktonic $\Delta^{14}C$ values in our marine records decrease by ~170‰. In the subtropical core at 18 kyr BP, the difference between the atmospheric signal and the *G. inflata* planktonic signal is 20‰ (slightly less than the modern value; Fig. 2c). Initially, the foraminiferal $\Delta^{14}C$ values decrease at a greater pace than atmospheric ^{14}C, such that at 16.2 kyr BP the difference between atmospheric and planktonic $\Delta^{14}C$ reaches 100–150‰ (Fig. 2b, c). After this, the planktonic $\Delta^{14}C$ record decreases more slowly whereas atmospheric ^{14}C decreases sharply, such that within the next 1.7 kyr (the period indicated by red shading on Fig. 2) the atmosphere–ocean difference is reduced almost to zero. The ^{14}C in SAMW (indicated by benthic foraminiferal $\Delta^{14}C$ in the Bay of Plenty core) largely mirrors the trend seen in planktonic $\Delta^{14}C$. At 18 kyr BP, SAMW is depleted by 150‰ relative to atmospheric values and decreases at a greater rate than the planktonics do until benthic ^{14}C is about 200‰ below the contemporaneous atmospheric values at 16.2 kyr BP. After this, SAMW $\Delta^{14}C$ plateaus until the ocean–atmosphere offset returns, between 15.0 and 14.5 kyr BP, to the value it had 18 kyr BP. AAIW, as recorded by benthic $\Delta^{14}C$ in our Chatham Rise core, displays fundamentally similar trends to the subtropical site. The planktonic $\Delta^{14}C$ record is analogous to the others, but shows oscillations and changing offsets among species from 17.8 to 16.5 kyr BP (Fig. 2b). These probably reflect variations in subsurface-to-surface and ocean-to-atmosphere carbon transfer and interspecies habitat differences. (See Supplementary Information for a full discussion.)

Our marine $\Delta^{14}C$ records support a southern locus as an exit route for CO_2 from a deep and isolated marine carbon reservoir during the early deglaciation, and help constrain the dynamics among the atmospheric CO_2 increase and $\Delta^{14}C$ decrease and the deglacial Southern Ocean degassing. Rapid CO_2 injection into the atmosphere begins

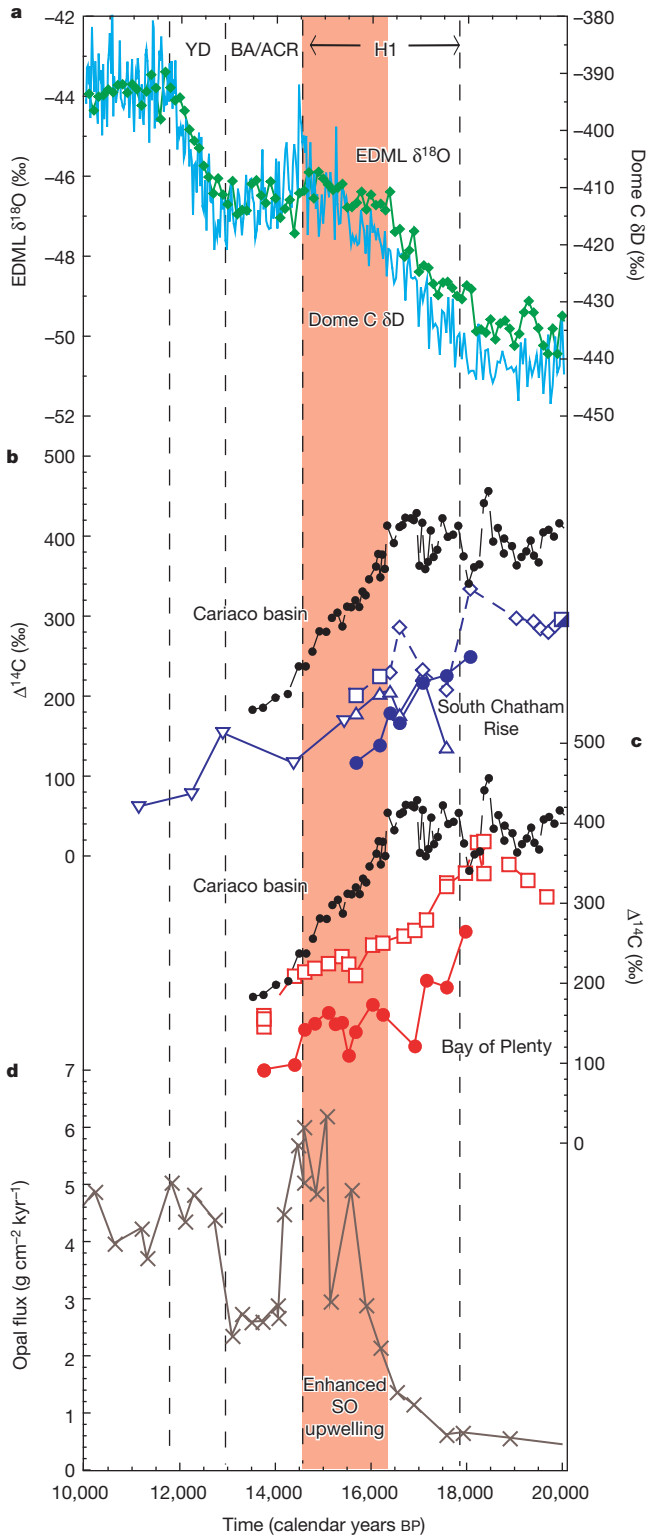

Figure 2 | Records of radiocarbon activities, Antarctic temperatures and Southern Ocean upwelling across the last deglaciation. **a**, Antarctic ice-core $\delta^{18}O$ ($[(^{18}O/^{16}O)_{sample}/(^{18}O/^{16}O)_{standard} - 1] \times 1{,}000$) from EDML (green[13]) and the hydrogen isotope deuterium (δD) from EPICA Dome C (light blue[2]), each of which is a temperature proxy, placed on the Greenland GISP2 timescale[5]. **b**, Atmospheric radiocarbon activities from the Cariaco basin (black), placed on the Hulu cave timescale[7], and south Chatham Rise marine $\Delta^{14}C$ from planktonic and benthic foraminifera (blue): *Globigerina bulloides* (planktonic; up-triangles show new data (this study); down-triangles show data from ref. 17), *Globorotalia inflata* (planktonic; squares), *Neogloboquadrina pachyderma* (s) (planktonic; diamonds), mixed *G. bulloides* and *N. pachyderma* (planktonic; half-open square), and mixed benthics (filled circles). **c**, Atmospheric radiocarbon activities from the Cariaco basin (black), placed on the Hulu cave timescale, and Bay of Plenty $\Delta^{14}C$ from core RR0503-JPC64 (red): *G. inflata* (planktonic; open squares) and mixed benthic foraminifera (closed circles). **d**, Opal fluxes, a proxy for upwelling south of the Antarctic polar front, from sediment core TN057-13-4PC (53.2° S, 5.1° E) in the Southern Ocean[4] (SO). The vertical dashed lines denote climatic intervals of the deglaciation as indicated at top: Heinrich event 1 (H1; timing as determined by reduced deep-water flux in the North Atlantic[24]), the Bølling–Allerød/Antarctic cold reversal (BA/ACR) and the Younger Dryas (YD). The shaded area corresponds to the period of enhanced upwelling in the Southern Ocean and the rapid drop in atmospheric $\Delta^{14}C$.

17.8 kyr BP[2], whereas the drastic drop in atmospheric $\Delta^{14}C$ begins later, ~16.5 kyr BP (Fig. 3a). The marine $\Delta^{14}C$ decrease starts 17.8 kyr BP, is concurrent with the initial rise in atmospheric CO_2 and leads the atmospheric ^{14}C decrease. Consequently, between 17.8 and 16.5 kyr BP the atmosphere/Southern Ocean isotopic difference increases by ~50‰. The change in offset across this time suggests that ^{14}C-depleted carbon upwelled into thermocline and surface waters in the Southern Ocean, but that air–sea exchange in the Southern Ocean was inadequate for that ^{14}C-depleted CO_2 to attain isotopic equilibration with the atmosphere. With constant air–sea mixing dynamics, the increase in atmospheric CO_2 concentration throughout this period would decrease surface marine $\Delta^{14}C$ relative to the atmospheric value (by ~10‰)[3,22], whereas higher air–sea exchange rates would minimize this effect. Thus, about 40‰ of the marine decrease may be attributed to injection of waters greatly depleted in ^{14}C relative to the atmosphere.

Starting around 16.5 kyr BP, increased opal fluxes at latitude 53° S (Fig. 2d) suggest substantial strengthening of Southern Ocean upwelling south of the Antarctic polar front[4] that increased marine biological productivity (also in evidence at our subpolar site; Fig. 3c). Coincident with the initiation of enhanced upwelling[4], the rate of atmospheric $\Delta^{14}C$ decrease accelerated[2] but radiocarbon levels in STMW, SAMW and possibly AAIW levelled out (Figs 2 and 3). Vigorous mixing and deeper convection[14] are plausible mechanisms to accelerate ^{14}C–^{12}C exchange and reduce the atmosphere–ocean $\Delta^{14}C$ difference. A concurrent release of highly ^{14}C-depleted CO_2 from the deep ocean would reduce the $\Delta^{14}C$ in both the atmosphere and the upper ocean. These interpretations make an implicit assumption that Pacific glacial and deglacial circulation was analogous to that today. Alternatively, it is possible that water upwelling in the Southern Ocean at this time was not significantly depleted in ^{14}C. Nonetheless, we suggest that deeper waters substantially depleted in ^{14}C were drawn to the upper layers in the Southern Ocean after 16.5 kyr BP (perhaps breaching a deep hydrologic front), and that vigorous exchange transferred the ^{14}C signal to the atmosphere. This caused the atmospheric $\Delta^{14}C$ value to drop rapidly and the Southern Ocean/atmosphere $\Delta^{14}C$ levels to become more closely aligned. At the start of the Antarctic cold reversal (~14.5 kyr BP), the atmosphere–ocean $\Delta^{14}C$ offset stabilized at the modern value (Fig. 2). This is attributed to Southern Ocean cooling that caused westerly winds to shift northwards, weakening upwelling[4]. This would have substantially damped ocean–atmosphere CO_2 and ^{14}C exchange in the region.

The relatively small maximum $\Delta^{14}C$ offset among the atmosphere, surface waters and subthermocline waters in the southwest Pacific (this study) and southeast Pacific[23] indicates there was substantial isotopic exchange with the atmosphere in the course of wind-driven upwelling and outgassing in the Southern Ocean. These results depart significantly from the large $\Delta^{14}C$ depletion reported from the eastern tropical North Pacific[5] (ETNP; Fig. 3b). In the ETNP, $\Delta^{14}C$ depletion began ~17.8 kyr BP, which precedes by ~1.7 kyr the onset of enhanced upwelling in the Southern Ocean[4] that is invoked to transport this signal to the ETNP. However, the depletion there is coincident with the onset of Heinrich event 1 and the collapse of NADW formation[24]. The position of the ETNP site in an eastern

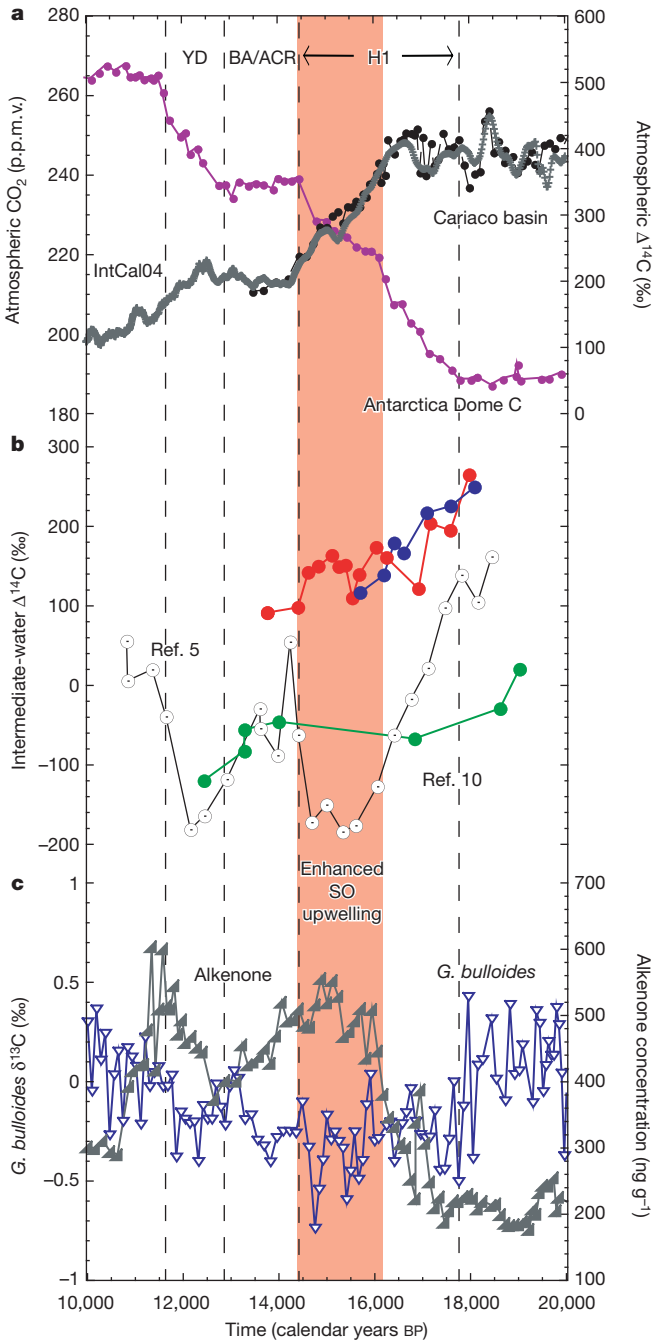

Figure 3 | Records of atmospheric CO_2, radiocarbon activities, and surface $\delta^{13}C$ and productivity across the last deglaciation. The initial deglacial rise in atmospheric CO_2 shown in the Southern Hemisphere ice-core records, the decrease in surface ocean $\delta^{13}C$ and the increase in alkenone productivity all coincide with the initial decrease in intermediate-water $\Delta^{14}C$. **a**, Atmospheric $\Delta^{14}C$ from the Cariaco basin (black[7]) and IntCal04 (grey[20]), and atmospheric CO_2 concentration from Antarctic ice core EPICA Dome C (purple[2]), placed on the GISP2 timescale[5]. **b**, Intermediate-water $\Delta^{14}C$ from south Chatham Rise core MD97-2120 (mixed benthics; blue circles), Bay of Plenty core RR0503-JPC64 (mixed benthics; red circles) and the Baja California ETNP site (mixed benthics; open circles[5]), and North Pacific deep-water $\Delta^{14}C$ (mixed benthics; green circles[10]). Although the three shallow sites show a decrease in $\Delta^{14}C$ beginning at ~17.8 kyr BP, only the tropical North Pacific site shows an extreme decrease in $\Delta^{14}C$, starting at the beginning of Heinrich event 1. **c**, MD97-2120 *G. bulloides* $\delta^{13}C$ (blue triangles[17]) and alkenone concentrations (grey triangles[32]) tuned to EDML. The alkenone concentrations are a measure of haptophyte productivity. The vertical dashed lines and the shaded area are as in Fig. 2.

boundary shadow zone makes subthermocline waters there sensitive to changes in steric height, thermocline depth[25] and internal mixing dynamics[26], which vary with subsurface water mass flux[27]. These would be sensitive to Northern Hemisphere thermohaline forcing. Also significant, the timing of the benthic $\Delta^{14}C$ decrease in the ETNP coincides with an oceanic ^{14}C plateau visible in marine fossils globally (~16.7–15.3 kyr BP)[28], which is attributed to global thermohaline reorganization. Expansion of a deep, poorly ventilated, ^{14}C-depleted North Pacific carbon reservoir with a different exit point, possibly the equatorial Pacific, could explain the ETNP $\Delta^{14}C$ value (Fig. 3b). An alternative interpretation for the $\Delta^{14}C$ difference between the ETNP and the South Pacific could be that CO_2 exiting through the Southern Ocean did not fully tap into an old carbon pool.

Notably, the initial $\Delta^{14}C$ decrease in marine records at ~18 kyr BP also coincides with the initial decrease in foraminifera $\delta^{13}C$ of the carbon isotope minimum event across the Southern and equatorial Pacific[4,16,29,30]. This event is generally interpreted as the entrainment of poorly ventilated, nutrient-rich waters from a glacial abyssal carbon pool. However, the absolute $\delta^{13}C$ minima at these widely dispersed sites are not contemporaneous, varying by 5 kyr (refs 4, 16, 29, 30), which points to local modification of any formation signal. The carbon isotope minimum event at our Southern Ocean (south Chatham Rise) site lasts from ~18 to 14 kyr BP (Fig. 3c).

Marine data from the southwest Pacific suggest a two-step ventilation of deep waters contributing CO_2 to the atmosphere. The initiation of the atmospheric CO_2 increase[2] coincided with a nearly total collapse of NADW formation in the subpolar North Atlantic[24] at the onset of Heinrich event 1, which affected density balances in waters outcropping in the Southern Ocean. We suggest that this brought CO_2-rich, ^{14}C-depleted water to the surface and that this water did not fully exchange isotopically with the atmosphere. Subsequent to this far-field forcing from the Northern Hemisphere, the ocean–atmosphere exchange in the Southern Ocean also responded to local forcing. Increasing Southern Ocean warmth[13] caused changes in wind placement[25,31], altering shallow-water formation and lateral pumping dynamics[14,27]. Models indicate that entrainment of waters sourced from mid-depths such as upper CPDW fundamentally affect surface ocean productivity and CO_2 levels[14]. Although our data do not address the absence of a significant change in the Pacific deep-water $\Delta^{14}C$ signal during the interval from 16.4 to 15.2 kyr BP[10,12], intensified pumping from moderate depths is consistent with the lack of a significant change in Pacific deep-water $\Delta^{14}C$ (refs 10, 12) through the early part of the deglaciation (17.8–16.2 kyr BP). The progressive shift of westerly winds to the south may have initiated a polar loop of shallow-water formation[14] that successively stripped CO_2 from mid-ocean depths before penetrating deeper into the ocean to release ^{14}C-depleted CO_2 from an older carbon reservoir. With moderate-depth waters as the main CO_2 source before the Antarctic cold reversal, the ^{14}C-depleted CO_2 released after the Antarctic cold reversal must have been from a smaller, more depleted reservoir that remains to be volumetrically constrained and chemically defined[12].

Received 19 October 2009; accepted 14 June 2010.

1. Toggweiler, J. R. Variation of atmospheric CO_2 by ventilation of the ocean's deepest water. *Paleoceanography* **14**, 571–588 (1999).
2. Monnin, E. *et al.* Atmospheric CO_2 concentrations over the last glacial termination. *Science* **291**, 112–115 (2001).
3. Broecker, W. & Barker, S. A 190‰ drop in atmosphere's $\Delta^{14}C$ during the "Mystery Interval" (17.5 to 14.5 kyr). *Earth Planet. Sci. Lett.* **256**, 90–97 (2007).
4. Anderson, R. F. *et al.* Wind-driven upwelling in the Southern Ocean and the deglacial rise in atmospheric CO_2. *Science* **323**, 1441–1448 (2009).
5. Marchitto, T., Lehman, S. J., Ortiz, J. D., Flückiger, J. & van Geen, A. Marine radiocarbon evidence for the mechanism of deglacial atmospheric CO_2 rise. *Science* **316**, 1456–1459 (2007).
6. Muscheler, R. *et al.* Changes in the carbon cycle during the last deglaciation as indicated by the comparison of ^{10}Be and ^{14}C records. *Earth Planet. Sci. Lett.* **219**, 325–340 (2004).
7. Hughen, K. A., Southen, J. R., Lehman, S. J., Bertrand, C. & Turnbull, J. Marine-derived ^{14}C calibration and activity record for the past 50,000 years updated from the Cariaco Basin. *Quat. Sci. Rev.* **25**, 3216–3227 (2006).

8. Robinson, L. F. *et al.* Radiocarbon variability in the western North Atlantic during the last deglaciation. *Science* **310,** 1469–1473 (2005).
9. Keigwin, L. D. Radiocarbon and stable isotope constraints on Last Glacial Maximum and Younger Dryas ventilation in the western North Atlantic. *Paleoceanography* **19,** PA4012 (2004).
10. Galbraith, E. D. *et al.* Carbon dioxide release from the North Pacific abyss during the last deglaciation. *Nature* **449,** 890–893 (2007).
11. Sikes, E. L., Samson, C. R., Guilderson, T. P. & Howard, W. R. Old radiocarbon ages in the southwest Pacific Ocean during the last glacial period and deglaciation. *Nature* **405,** 555–559 (2000).
12. Broecker, W., Clark, E. & Barker, S. Near constancy of the Pacific Ocean surface to mid-depth radiocarbon-age difference over the last 20 kyr. *Earth Planet. Sci. Lett.* **274,** 322–326 (2008).
13. EPICA. One-to-one coupling of glacial climate variability in Greenland and Antarctica. *Nature* **444,** 195–198 (2006).
14. Toggweiler, J. R., Russell, J. L. & Carson, J. R. Mid-latitude westerlies, atmospheric CO_2, and climate changes during the ice ages. *Paleoceanography* **21,** PA2005 (2006).
15. Hanawa, K. & Talley, L. D. in *Ocean Circulation and Climate* (eds Seidler, G., Church, J. & Gould, J.) 373–386 (Int. Geophys. Ser., Academic, 2001).
16. Bostok, H. C., Opdyke, B. N., Gagan, M. K. & Fifield, L. K. Carbon isotope evidence for changes in Antarctic Intermediate Water circulation and ocean ventilation in the southwest Pacific during the last deglaciation. *Paleoceanography* **19,** PA4013 (2004).
17. Pahnke, K., Zahn, R., Elderfield, H. & Schulz, M. 340,000 year centennial scale marine record of southern hemispheric climate oscillation. *Science* **301,** 948–952 (2003).
18. Shane, P. A., Sikes, E. L. & Guilderson, T. P. Tephra beds in deep-sea cores off northern New Zealand: implications for the history of Taupo Volcanic Zone, Mayor Island, and White Island volcanoes. *J. Volcanol. Geotherm. Res.* **154,** 276–290 (2006).
19. Lowe, D. J., Shane, P. A. R., Alloway, B. V. & Newnham, R. W. Fingerprints and age models for widespread New Zealand tephra marker beds erupted since 30,000 yr ago as a framework for NZ-INTIMATE. *Quat. Sci. Rev.* **27,** 95–126 (2008).
20. Reimer, P. J. *et al.* IntCal04 terrestrial radiocarbon calibration, 0–26 cal kyr BP. *Radiocarbon* **46,** 1029–1058 (2004).
21. Key, R. M. *et al.* WOCE AMS radiocarbon I: Pacific Ocean results (P6, P16, and P17). *Radiocarbon* **38,** 425–518 (1996).
22. Bard, E. Correction of accelerator mass spectrometry ^{14}C ages measured in planktonic foraminifera: paleoceanographic implications. *Paleoceanography* **3,** 635–646 (1988).
23. Pol-Holz, R. D., Keigwin, L., Southon, J., Hebbeln, D. & Mohtadi, M. No signature of abyssal carbon in intermediate waters off Chile during deglaciation. *Nature Geosci.* **3,** 192–195 (2010).
24. McManus, J. F., Francois, R., Gherardi, J. M., Keigwin, L. D. & Leger, S. B. Collapse and rapid resumption of Atlantic meridional circulation linked to deglacial climate changes. *Nature* **428,** 834–837 (2004).
25. Gnanadesikan, A., Russell, J. L. & Zeng, F. How does ocean ventilation change under global warming? *Ocean Sci.* **3,** 43–53 (2007).
26. Curry, W. B. & Oppo, D. Glacial water mass geometry and the distribution of $\delta^{13}C$ of ΣCO_2 in the Western Atlantic Ocean. *Paleoceanography* **20,** PA1017 (2005).
27. Gnanadesikan, A. A simple model for the structure of the oceanic pycnocline. *Science* **283,** 2077–2079 (1999).
28. Sarnthein, M., Grootes, P. M., Kennett, J. P. & Nadeau, M.-J. in *Ocean Circulation: Mechanisms and Impacts* (eds Schmittner, A., Chiang, J. C. H. & Hemmings, S. R.) 175–196 (Geophys. Monogr. Ser. 173, American Geophysical Union, 2007).
29. Pahnke, K. & Zahn, R. Southern hemisphere water mass conversion linked with North Atlantic climate variability. *Science* **307,** 1741–1746 (2005).
30. Spero, H. J. & Lea, D. W. The cause of carbon isotope minimum events on glacial terminations. *Science* **296,** 522–525 (2002).
31. Russell, J. L., Dixon, K. W., Gnanadesikan, A., Stouffer, R. J. & Toggweiler, J. R. Southern Ocean westerlies in a warming world: propping open the door to the deep ocean. *J. Clim.* **19,** 6382–6390 (2006).
32. Sachs, J. P. & Anderson, R. F. Increased productivity in the Subantarctic ocean during Heinrich events. *Nature* **434,** 1118–1120 (2005).

Supplementary Information is linked to the online version of the paper at www.nature.com/nature.

Acknowledgements We thank the captain and crew of the RV *Revelle*, and our shipboard colleagues during the Zheng leg 3 (RR0503) cruise funded by the National Science Foundation (NSF), which collected the RR core. Core MD97-2120 was collected through the International Marine Past Global Change Study (IMAGES) program and with the technical support of the Institut Polaire Français Paul Emile Victor (IPEV) who made the research vessel Marion Dufresne available for core retrieval. H.J.S., E.L.S. and T.P.G., and the shore analyses, were supported by NSF awards and the Evolving Earth Foundation, and the Geological Society of America provided support for K.A.R. during her MSc. R.Z. acknowledges support from the MICINN, Spain. A portion of this work was performed under the auspices of the US Department of Energy by Lawrence Livermore National Laboratory. We especially thank M. Cook for discussions, continuing input and suggestions throughout this study.

Author Contributions K.A.R. participated in the RR0503 cruise, sampled cores, prepared sediments, speciated foraminifera for isotopic and radiocarbon analyses, performed all stable isotopic analyses and prepared figures. E.L.S. led the RR0503 cruise, sampled cores, speciated foraminifera for isotopic and radiocarbon analyses, prepared figures and wrote the paper. T.P.G. participated in the RR0503 cruise and performed all radiocarbon analyses. P.S. participated in the RR0503 cruise and identified all tephras. H.J.S. designed the study and, with T.M.H., supervised KAR during her MSc. R.Z. provided the MD core samples and supplementary data for that core. All authors contributed to the interpretation of the results and provided input on the manuscript.

Author Information Reprints and permissions information is available at www.nature.com/reprints. The authors declare no competing financial interests. Readers are welcome to comment on the online version of this article at www.nature.com/nature. Correspondence and requests for materials should be addressed to E.L.S. (sikes@marine.rutgers.edu).

SUPPLEMENTARY INFORMATION

SI #1 Sample preparation and analyses

New planktonic and benthic foraminiferal radiocarbon ages were generated for late glacial and deglacial intervals from two shallow cores (**Table S1**). Core RR0503 JPC 64 (37° 25.34′S 177° 00.41′E and 651 m depth) is from the Bay of Plenty, northern New Zealand in the subtropical South Pacific and core MD97-2120 (43° 32.06′S 174° 55.85′E and 1210 m depth) is from sub-Antarctic waters on the South Chatham Rise of New Zealand. Bulk sediment samples were disaggregated from both cores with deionized water, wet sieved through a 63 μm sieve, and dried in an oven at 45°C. Prior to washing, the wet sediment from core RR0503-64 was oven-dried at 45°C to determine the sample dry weight. Single species of planktonic foraminifera were picked for both radiocarbon and stable isotopes from the >150μm fraction. In MD-97-2120 *Globigerina bulloides*, and *Neogloboquadrina pachyderma* (s) were picked. In RR0503-64 *G. bulloides* and *Globorotalia inflata* were selected. For both cores, fossil *G. bulloides* shells were picked from the 150-250 μm and 250-350 μm sieve fractions. We then measured the length of each specimen with a reticulated ocular microscope and separated the specimens into a size bin of 267-333 μm[1]. For core MD97-2120, *N. pachyderma (s)* were picked from the 150-250 μm size fraction; for core RR0503-64, *G. inflata* shells were picked from the 250-350 μm and >350 μm size fraction and then pooled for analysis. The benthic species *Uvigerina perigrina* was picked for stable isotopes and mixed benthics were selected for radiocarbon analyses in both cores. After picking, the tests were briefly sonicated in methanol. Stable oxygen and carbon isotopes were run on individual species in the UC Davis Department of Geology stable isotope laboratory. Prior to analysis the samples were roasted *in vacuo* for 30 minutes at 375ºC and then analyzed using an Isocarb common acid bath autocarbonate device attached to a Fisons Optima isotope ratio mass spectrometer. Values are reported in ‰ notation relative to the PDB (Vienna Pee Dee Belemnite) standard. Analytical precision was 0.05 ‰ for $\delta^{18}O$ and 0.04 ‰ for $\delta^{13}C$ ($\pm 1\ \sigma$) based on repeated analyses of an in-house marble standard, UCD-SM92.

Clean foram samples for radiocarbon analyses were chemically leached, converted to CO_2 and graphitized prior to AMS-^{14}C analysis at Lawrence Livermore Center for Accelerator Mass Spectrometry (CAMS). When samples were large enough, forams were physically cracked and sonicated in methanol prior to leaching. δ^{13}C corrections were derived from stable isotope analyses on the same samples. ^{14}C calculations were based on the conventions of Stuiver and Polach[2].

SI #2 Age Models for the cores

MD97-2120

The original age model of core MD97-2120 was derived from ^{14}C dating 0-22,000 years[3] and correlating its temperature-sensitive planktonic foraminiferal trace element record with the deuterium record from the Antarctic Vostok ice core[3] for older sediments. In this study we focus on the uppermost section of the record, from 10,000-22,000 ybp, and modified the originally published age model through this section by using *G. bulloides* δ^{18}O between 13,000-19,000 ybp to produce a calendar –age model based on the correlation of planktonic δ^{18}O at 2 cm resolution with the δ^{18}O from the EPICA Dronning Maud Land (EDML) ice core[4] (**Table S2 and Figure S1a)**. This revised age model was necessary to provide a ^{14}C -independent stratigraphy through this critical time period, so that the use of ^{14}C as a tracer is not biased by using it as a stratigraphic tool across this short time frame. Radiocarbon dates used in this study for stratigraphy were converted to calendar ages using the planktonic ^{14}C data and applying the Calib v. 5.0.1 and MARINE04 calibration program. This re-adjustment provides sedimentation rates that are consistent throughout the core and are ~20 to 24 cm/ky through the time interval of interest (**Table S2 and Figure S2a**). Changes in the δ^{18}O of MD97-2120 covary with changes in the EDML ice core. For example: the large decrease in the *G. bulloides* δ^{18}O corresponds to the initial increase in EDML δ^{18}O around 18 ka (**Figure S1a)**. Importantly, the calendar ages based on the independent age scales are generally in excellent agreement with the previously published age model[3,5].

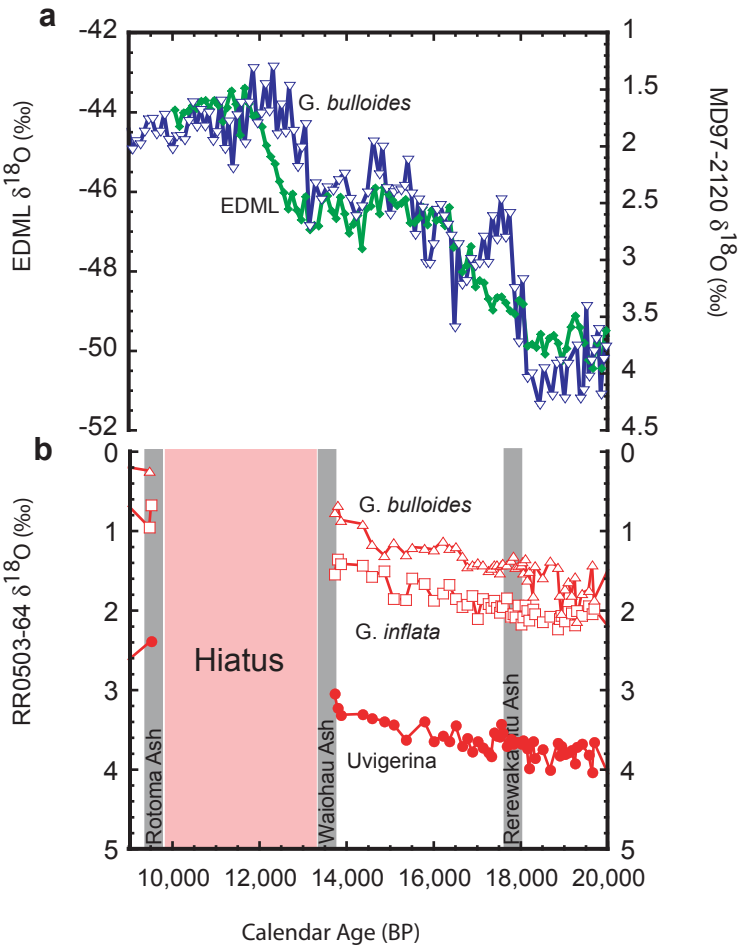

Figure S1.
(a) Antarctic ice core record of $\delta^{18}O$ from EDML (green) [4] and *G. bulloides* $\delta^{18}O$ from South Chatham Rise core MD97-2120 [3] tuned to EDML $\delta^{18}O$. **(b)** $\delta^{18}O$ from Bay of Plenty core RR0503-64. *G. bulloides* (triangles), *G. inflata* (squares), *Uvigerina sp.* (closed circles).

RR0503 JPC-64

The age model for core RR0503-JPC-64 (37° 25.34′S 177° 00.41′E and 651 m depth) in the Bay of Plenty was developed by combining calendar age model tie points from tephra chronology in the core[6] with planktonic $\delta^{18}O$ stratigraphy. The tephra chronology is tied to established New Zealand chronologies based on ^{14}C dating of terrestrial material and statistically fit to calendar ages[7-8] (**Figure S1b)**. The presence of the Whakatane (5.5±0.06 cal kyr BP) tephra at 37 cm overlying the Rotoma (9.5±0.03 cal kyr BP) implies continuous sedimentation at a rate of~13 cm/ka above this ash. The presence of the Rotoma and Waiohau (13.6±0.03 cal kyr BP) [7] tephras directly overlying each other at 88-90 and 91-93 cm indicate a hiatus of ~4,100 years (**Figure S2b)**. The timing of this hiatus is coincident with a still-stand in sea level rise between the two well known deglacial meltwater pulses. In New Zealand this is a period with widespread climate changes detected in North Island terrestrial sedimentation patterns and pollen assemblages that are interpreted to represent more "unsettled weather". These conditions immediately follow (and stratigraphically would lie directly above) the Waiohau tephra[9]. Such conditions may have contributed to changed sedimentation conditions offshore causing the hiatus. ^{14}C samples taken through the Rotoma ash with ages substantially older than the established age of that tephra, confirm the presence of a hiatus prior to the placement of the ash (**Table S1**).

The presence of the Rerewakaaitu ash (17.6±0.4 cal kyr BP)[7] at 151-154 cm (58 cm below the Waiohau) suggests continuous sedimentation at a rate ranging from 14 to 26 cm/kyr through the time period of interest (**Table S3**). The $\delta^{18}O$ record of the three species (planktonics *G. bulloides*, *G. inflata* and benthic *Uvigerina, sp.*) between the Waiohau and the Rerewakaaitu ash indicate continuous sedimentation throughout the period of interest in this core (**Figure S1b)** and provide a stratigraphic tie point through the crucial time period in the core. In RR0503 JPC64, $\delta^{18}O$ stratigraphy is at 2 cm resolution from 0-210 cm (**Table S3**). The deglacial interval of depleted radiocarbon activity that we report appears as age plateaus and planktonic-benthic reversals in the conventional age: depth relationship (**Table S1**). Mass inputs such as slumps could theoretically produce such a phenomenon, however, the $\delta^{13}C$ and $\delta^{18}O$ in the core show no

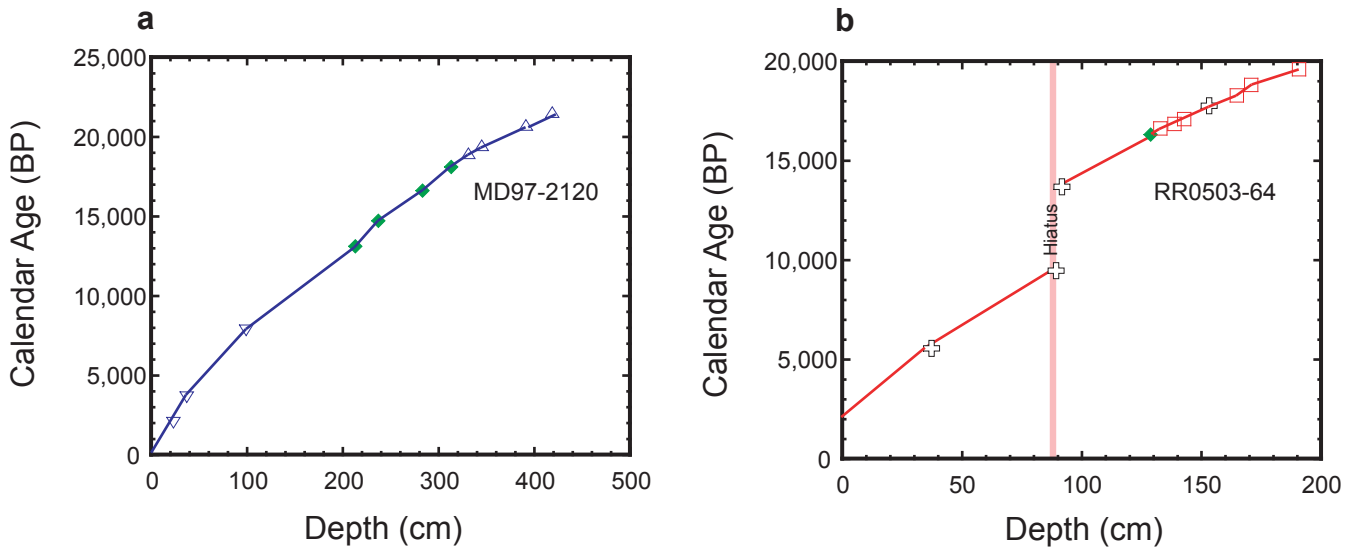

Figure S2 **Age model for cores in this study**
(a) Age model for core MD97-2120. Calendar age tie points for G .bulloides ^{14}C ages (blue triangles; this study) $\Delta^{14}C$ from *G. bulloides* (upside down triangles [3]), G. inflata (squares, this study) $\delta^{18}O$ adjusted to $\delta^{18}O$ from EDML (green diamonds) **(b)** Age model for core RR0503-JPC64. Calendar age tie points for *G. inflata* (squares), tephra (open crosses) and $\delta^{18}O$ adjusted to $\delta^{18}O$ from EDML (green diamonds) plotted against depth in core. The presence of the Rotoma and Waihau[7] tephras directly overlying each other at 89-90 and 90.5-91.5 cm indicate a hiatus of ~4,100 years (see supplementary information text). The presence of the Rerewakaaitu ash 7 at 151-154 cm (62 cm below the Waiohau) suggests continuous sedimentation through the time period of interest. We fit a linear age vs. depth regression for the data above and below the hiatus and corrected all *G. inflata radiocarbon* dates using a marine reservoir age (ΔR) of -50 ± 40 years, based on local modern reservoir ages[11]

anomalous shifts (**Figure S1b)** and the sedimentation rate through this period is similar to that before (14 cm/kyr) and after (~13 cm/kyr) the hiatus (**Table S3**) .

SI#3 Stratigraphic Age Model Constraints on Radiocarbon Results

The effect of stratigraphy on the paleo $\Delta^{14}C$ is a valid concern especially when correlating $\delta^{18}O$ between different sources such as ice cores and microfossils from marine sediment. The choice of tie points when developing correlations becomes critical in producing a robust age model. To examine the magnitude of this effect, we developed an alternate stratigraphy for each core based on alternate, but equally viable choices of $\delta^{18}O$ pattern matches to the EDML[4] (**Table S4**) and plotted both stratigraphies against atmospheric paleo $\Delta^{14}C$ (**Figure S3**).

Changes to the independent age model in these cores would affect the designated age of a sample relative to the other independent data streams such as atmospheric ^{14}C and CO_2 content. However, the chosen age model does not directly affect marine paleo- $\Delta^{14}C$ calculations. The determination of the paleo- $\Delta^{14}C$ for each time point in the past was calculated using internally consistent values from within the ^{14}C data. The absolute $\Delta^{14}C$ is calculated according to convention[2] from which $\Delta^{14}C$ was converted to age in radiocarbon years according to convention (using the Libby half life of ^{14}C)[2]. Conversion to the corresponding calendar age was via the Calib v. 5.0.1 program and MARINE04 [10] (**Table S1**). This yields a "calibrated" calendar age. The resulting calendar age and the fraction modern are used to obtain the paleo $\Delta^{14}C$. The independently obtained age model (see above) is used as the down core age of the resulting paleo $\Delta^{14}C$ values.

Changes in age determinations within the cores is governed by correlation picks. Our analysis demonstrates that the application of subtly different stratigraphies for paleo-$\Delta^{14}C$ interpretations has little effect on RR0505 JPC 64 (**Figure S3 c&d**). There is a slightly greater impact of subtly different stratigraphies on core MD97-2120. The choice of correlation picks between the EDML and MD97-2120 $\delta^{18}O$ affected age determinations for an individual sample depth by as few as 1year and as many as 530 years (average 219 years). Offsets primarily affect the planktonic data younger than 15,000 years (**Figure S3a&b)**. Importantly, the choice of stratigraphy does not change the ages of individual points enough to affect interpretations in this study.

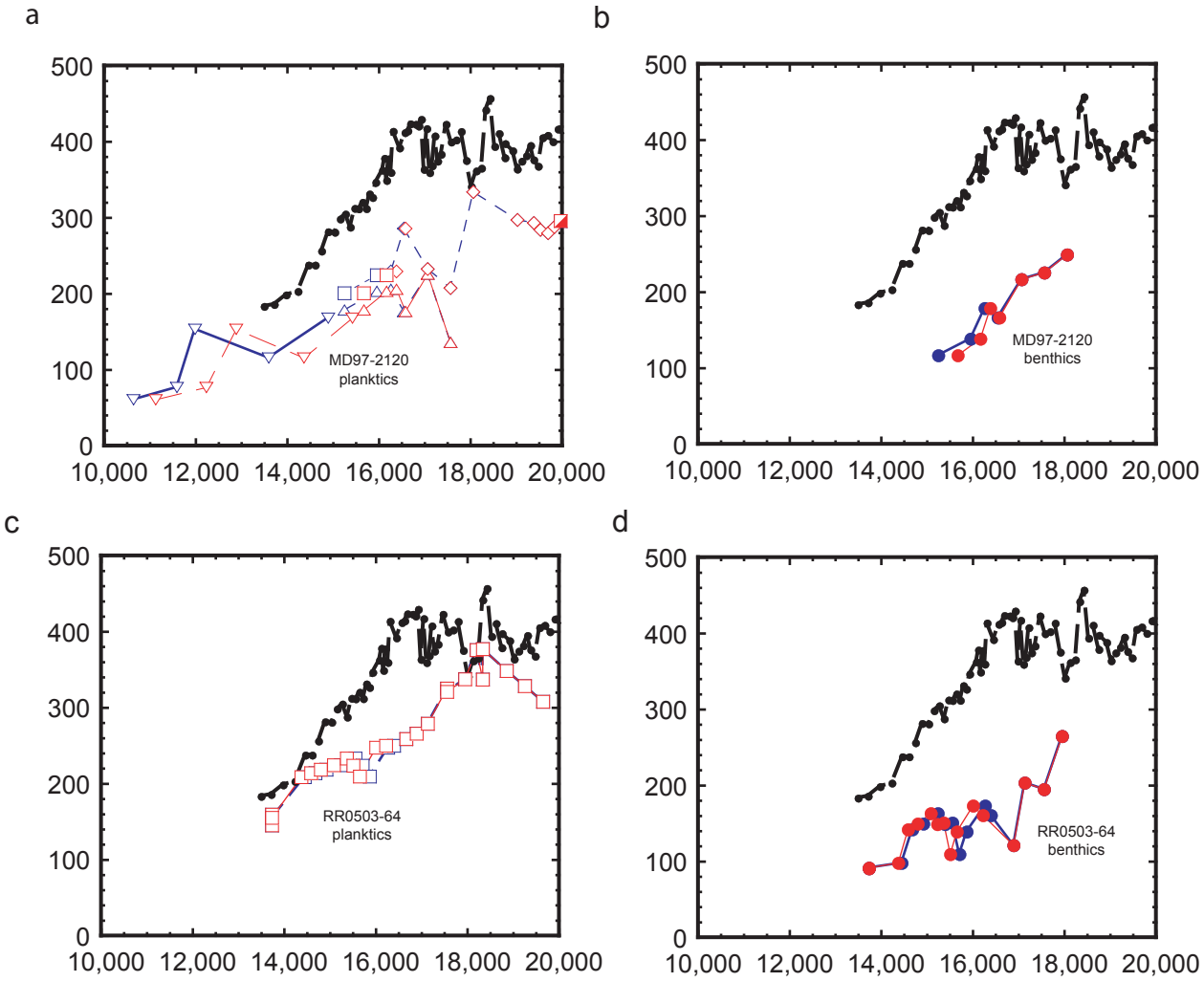

Figure S3 **Effect of alternate age models on $\Delta^{14}C$ calculations for the cores in this study (a)** Core MD97-2120 planktonic data with stratigraphy used in this paper in red symbols (triangles; this study), *G. bulloides* (upside down triangles [3]), *G. inflata* (squares, this study) and the alternative stratigraphy in blue symbols. **(b)** Core MD97-2120 benthic data with stratigraphy used in this paper in red circles and the alternative stratigraphy, blue circles. **(c)** Core RR0503-JPC64 planktonic data with stratigraphy used in this paper in red squares and the alternative stratigraphy in blue squares. **(d)** Core RR0503-JPC64 benthic data with stratigraphy used in this paper in red circles and the alternative stratigraphy, blue circles.

SI#4 Constraints on benthic and planktonic data points at the Southern Ocean site.

$\Delta^{14}C$ in our Southern Ocean site displays fundamentally similar trends to the subtropical site. However, the planktonic $\Delta^{14}C$ shows oscillations and variation between species from 17.8 to 16.5 ka that are not present in our other marine records (**Figure S3a and Figure 2b**). The variations between the two planktonic species on which our $\Delta^{14}C$ were based suggest that conditions controlling the radiocarbon content in surface waters were highly variable through this period. *G. bulloides* and *N. pachyderma* in this region have been shown to be offset both in their season of growth and depth habitat[11]. In several samples the planktonic *G. bulloides* and benthic $\Delta^{14}C$ are essentially the same. This is indicative of deep mixing, equilibrium between surface and shallow subsurface waters, and/or rapid lateral transport of AAIW from the zone of entrainment to the Chatham Rise. For one sample at 17.5 ka, the planktonic species *G. bulloides* has more a depleted $\Delta^{14}C$ that the benthics. There are several possible explanations for this that may have worked singly or in concert:

First, seasonal conditions such as sea ice extent, deep mixing and degassing may have been variable, coinciding with the initial increase in atmospheric pCO_2[12] and initial warming in Antarctica, and pre-dating the onset of sustained upwelling[13] in the Southern Ocean. It has been shown that the mixed layer can deepen in some sectors and shoal in other regions of the Southern Ocean in response to changes in wind intensification which can make air sea exchange zonally heterogeneous[14]. These zonal differences can vary on short (interannual) timescales. These dynamics would have affected local atmosphere –ocean $\Delta^{14}C$ exchange with the result that subsurface-to-surface $\Delta^{14}C$ balances may have been affected. This in turn may have cause the waters (shallower than ~300 m) in which *G. bulloides* grew to have had lower $\Delta^{14}C$ content than waters that were entrained further south (and to the west) into AAIW at that time. This could occur if waters that upwelled further south in the winter released their $\Delta^{14}C$ depleted CO_2 more effectively when they were entrained than the waters at the surface to the Chatham Rise in which our planktonics grew. Although we make an implicit assumption that Pacific glacial and deglacial circulation was analogous to today we cannot preclude that circulation may have been different in the past.

Second, planktonic foraminifera in this area have a narrow season of growth (up to 90% of the flux can occur in 2 weeks)[15] whereas benthic foraminifera can live for over a year. The two may

be integrating different timescales into their tests. If entrainment and surface mixing conditions were variable or patchy[14] across seasons, reversals could be caused by differential sampling of existing conditions by the different taxa.

Finally, differential bioturbation of the benthic and planktonic populations cannot be discounted. Although the high sedimentation rate in this core (around 20 cm/ka for this portion) should minimize biasing[16], changes in abundance will have an effect on radiocarbon ages[17]. Below this particular sample, the abundances of *G. bulloides* were too low to obtain sufficient numbers to obtain a single species analysis.

References

1 Spero, H. J. & Lea, D. W. Experimental determination of stable isotope variability in *Globigerina bulloides*: implications for paleoceanographic reconstructions. *Mar. Micropaleontol.* **28**, 231-246 (1996).

2 Stuiver, M. & Polach, H. A. Discussion and reporting of ^{14}C data. *Radiocarbon* **19**, 355-363 (1977).

3 Pahnke, K., Zahn, R., Elderfield, H. & Schulz, M. 340,000 year centennial scale marine record of southern hemispheric climate oscillation. *Science* **301**, 948-952 (2003).

4 EPICA. One-to-one coupling of glacial climate variability in Greenland and Antarctica. *Nature* **444**, 195-198 (2006).

5 Pahnke, K. & Zahn, R. Southern hemisphere water mass conversion linked with North Atlantic climate variability. *Science* **307**, 1741-1746 (2005).

6 Shane, P. A., Sikes, E. L. & Guilderson, T. P. Tephra beds in deep-sea cores off northern New Zealand: implications for the history of Taupo Volcanic Zone, Mayor Island, and White Island volcanoes. *Journal of Volcanic and Geothermal Research* **154**, 276-290 (2006).

7 Lowe, D. J., Shane, P. A. R., Alloway, B. V. & Newnham, R. W. Fingerprints and age models for widespread New Zealand tephra marker beds erupted since 30,000 yr ago as aframework for NZ-INTIMATE. *Quaternary Science Reviews* **27**, 95-126 (2008).

8 Alloway, B. V. *et al.* Towards a climate event stratigraphy for New Zealand over the past 30 000 years (NZ-INTIMATE project). *Journal of Quaternary Science* **22**, 9-35 (2007).

9 Newnham, R. M. & Lowe, D. J. Fine resolution pollen record of late glacial climate reversal from New Zealand. *Geology* **28**, 759-762 (2000).

10 Reimer, P. J. *et al.* IntCal04 Terrestrial radiocarbon calibration, 0-26 Cal Kyr BP. *Radiocarbon* **46**, 1029-1058 (2004).

11 King, A. L. & Howard, W. R. Planktonic foraminiferal flux seasonality in Subantarctic sediment traps: a test for paleoclimatic reconstructions. *Paleoceanography* **18**, doi:10.0129/2002PA000839 (2003).

12 Monnin, E. *et al.* Atmospheric CO_2 Concentrations over the Last Glacial Termination. By:. *Science* **291**, 112- 115 (2001).

13 Anderson, R. F. *et al.* Wind-driven upwelling in the Southern Ocean and the deglacial rise in atmospheric CO_2. *Science* **323**, 1441-1448 (2009).

14 Sallée, J. B., Speer, K. G. & Rintoul, S. R. Zonally asymmetric response of the Southern Ocean mixed layer depth to the Southern Annular Mode *Nature Geosci.* **3**, 273-279 (2010).

15 King, A. L. & Howard, W. R. Seasonality of foraminiferal flux in sediment traps at Chatham Rise, SW Pacific: implications for paleotemperature estimates. *Deep-Sea Research I* **48**, 1687-1708 (2001).

16 Guinasso, N. L. J. & Shink , D. R. Quantitative estimates of biological mixing rates in abyssal sediments. *Journal of Geophysical Research* **80**, 3032-3043 (1975).

17 Peng, T.-S. & Broecker, W. S. The impacts of bioturbation on the age difference between benthic and planktonic foraminifera in deep sea sediments. *Nuclear Instruments and Methods in Physics Research* **B5**, 346-352 (1984).

18 Sikes, E. L., Samson, C. R., Guilderson, T. P. & Howard, W. R. Old radiocarbon ages in the southwest Pacific Ocean during the last glacial period and deglaciation. *Nature* **405**, 555-559 (2000).

Table S1. **Compiled radiocarbon data RR0503-64 & MD97-2120 data**

CAMS #	Core	Species	Depth (cm)	Fraction Modern	±	$\Delta^{14}C$ (per mil)	±	^{14}C age (yr BP)	±	Calibrated Calendar Age (yr BP)
126162	RR0503-64	G. *inflata*	76-78	0.3007	0.0010	-699	1	9650	30	10553
123744	RR0503-64	G. *inflata*	87-89	0.2424	0.0013	-758	1	11385	45	12946
123751	RR0503-64	mixed benthics	87-89	0.2245	0.0011	-776	1	12000	45	13149
124647	RR0503-64	G. *inflata*	88-90	0.2275	0.0008	-772	1	11895	30	13368
124653	RR0503-64	mixed benthics	88-90	0.2422	0.0016	-758	2	11390	60	12718
124646	RR0503-64	G. *inflata*	90-91	0.2057	0.0007	-794	1	12700	30	14269
124652	RR0503-64	mixed benthics	90-91	0.1976	0.0007	-802	1	13030	35	14131
123745	RR0503-64	G. *inflata*	90-92	0.2053	0.0011	-795	1	12720	45	14316
123754	RR0503-64	G. *inflata*	90-92	0.2122	0.0013	-788	1	12450	50	13941
123752	RR0503-64	mixed benthics	90-92	0.2003	0.0012	-800	1	12915	50	14019
141045	RR0503-64	G. *inflata*	100-101	0.1960	0.0013	-804	1	13090	60	15041
141050	RR0503-64	mixed benthics	100-101	0.1970	0.0017	-803	2	13050	70	14208
141046	RR0503-64	G. *inflata*	103-104	0.1899	0.0018	-810	2	13350	80	15341
141051	RR0503-64	mixed benthics	103-104	0.1884	0.0022	-812	2	13410	100	14899
141047	RR0503-64	G. *inflata*	106-107	0.1867	0.0014	-813	1	13480	60	15510
141048	RR0503-64	mixed benthics	106-107	0.1851	0.0022	-815	2	13550	100	15104
140239	RR0503-64	G. *inflata*	110-111	0.1843	0.0014	-816	1	13580	60	15658
140240	RR0503-64	mixed benthics	110-111	0.1770	0.0051	-823	5	13910	240	15567
141049	RR0503-64	mixed benthics	112-113	0.1850	0.0017	-815	2	13550	80	15100
140241	RR0503-64	G. *inflata*	114-115	0.1815	0.0009	-818	1	13710	45	15844
140242	RR0503-64	mixed benthics	114-115	0.1825	0.0013	-818	1	13660	60	15229
140243	RR0503-64	G. *inflata*	116-117	0.1845	0.0015	-815	1	13570	70	15643
140244	RR0503-64	mixed benthics	116-117	0.1951	0.0021	-805	2	13130	90	14375
142199	RR0503-64	G. *inflata*	118-119	0.1926	0.0011	-807	1	13235	50	15196
142200	RR0503-64	mixed benthics	118-119	0.1874	0.0036	-813	4	13450	160	14926
124644	RR0503-64	G. *inflata*	123-124	0.1747	0.0008	-825	1	14015	40	16253
124650	RR0503-64	mixed benthics	123-124	0.1727	0.0015	-827	1	14110	70	15842
124645	RR0503-64	G. *inflata*	126-127	0.1729	0.0007	-827	1	14095	35	16355
124651	RR0503-64	mixed benthics	126-127	0.1769	0.0018	-823	2	13910	90	15554
126160	RR0503-64	G. *inflata*	132-133	0.1680	0.0007	-832	1	14325	40	16651
127313	RR0503-64	G. *inflata*	138-139	0.1644	0.0009	-836	1	14505	50	16880
127312	RR0503-64	mixed benthics	138-139	0.1579	0.0029	-842	3	14830	150	16209
126161	RR0503-64	G. *inflata*	142-143	0.1613	0.0007	-839	1	14660	40	17122
127311	RR0503-64	mixed benthics	142-143	0.1571	0.0019	-843	2	14870	100	16835
123746	RR0503-64	G. *inflata*	148-150	0.1541	0.0010	-846	1	15020	60	17791
123755	RR0503-64	G. *inflata*	148-150	0.1554	0.0010	-845	1	14960	50	17698
123753	RR0503-64	mixed benthics	148-150	0.1619	0.0011	-838	1	14630	60	16529
124639	RR0503-64	G. *inflata*	155-157	0.1499	0.0007	-850	1	15245	40	18095
124649	RR0503-64	mixed benthics	155-157	0.1452	0.0007	-855	1	15500	40	17895
124640	RR0503-64	G. *inflata*	161-162	0.1487	0.0007	-851	1	15310	40	18396
123747	RR0503-64	G. *inflata*	164-165	0.1471	0.0010	-853	1	15400	60	18249
123756	RR0503-64	G. *inflata*	164-165	0.1489	0.0010	-851	1	15300	60	18395
124641	RR0503-64	G. *inflata*	170-171	0.1380	0.0007	-862	1	15910	40	18846
124642	RR0503-64	G. *inflata*	180-181	0.1334	0.0007	-867	1	16180	40	19002
124643	RR0503-64	G. *inflata*	190-191	0.1217	0.0006	-878	1	16920	45	19638
124648	RR0503-64	G. *inflata*	200-201	0.1223	0.0006	-878	1	16875	45	19729
Pahnke et al. (2003)	MD97-2120	G. *bulloides*	22.5	0.7250		-65		2585		2058
Pahnke et al. (2003)	MD97-2120	G. *bulloides*	36.5	0.6157		-37		3895		3664
Pahnke et al. (2003)	MD97-2120	G. *bulloides*	98.5	0.3903		27		7560		7869
Pahnke et al. (2003)	MD97-2120	G. *bulloides*	168.5	0.2690		43		10550		11346
Pahnke et al. (2003)	MD97-2120	G. *bulloides*	192.5	0.2656		176		10650		11576
Pahnke et al. (2003)	MD97-2120	G. *bulloides*	202.5	0.2468		161		11240		12750
Pahnke et al. (2003)	MD97-2120	G. *bulloides*	230.5	0.2066		110		12665		13945
Pahnke et al. (2003)	MD97-2120	G. *bulloides*	252.5	0.1945		180		13155		14824
120237	MD97-2120	G. *bulloides*	258-259	0.1871	0.0011	-813	1	13465	50	15221
141053	MD97-2120	G. *inflata*	258-259	0.1769	0.0008	-823	1	13915	40	15837
140228	MD97-2120	mixed benthics	258-259	0.1767	0.0010	-823	1	13925	45	15245
120238	MD97-2120	G. *bulloides*	270-271	0.1759	0.0010	-824	1	13960	50	15898

141052	MD97-2120	G. *inflata*	270-271	0.1648	0.0008	-835	1	14480	40	16580
140229	MD97-2120	mixed benthics	270-271	0.1662	0.0016	-834	2	14410	80	15911
120240	MD97-2120	G. *bulloides*	275-276	0.1746	0.0010	-825	1	14020	50	15980
124654	MD97-2120	mixed benthics	275-276	0.1488	0.0007	-851	1	15305	45	17114
120239	MD97-2120	N. *pachyderma*	275-276	0.1620	0.0020	-838	2	14620	100	16760
120242	MD97-2120	G. *bulloides*	280-281	0.1905	0.0011	-810	1	13320	45	15059
124655	MD97-2120	mixed benthics	280-281	0.1524	0.0007	-848	1	15115	40	16830
120241	MD97-2120	N. *pachyderma*	280-281	0.1513	0.0014	-849	1	15170	80	17695
120244	MD97-2120	G. *bulloides*	290-291	0.1640	0.0010	-836	1	14520	50	16632
124656	MD97-2120	mixed benthics	290-291	0.1433	0.0007	-857	1	15605	45	17687
120243	MD97-2120	N. *pachyderma*	290-291	0.1602	0.0017	-840	2	14710	90	16873
120246	MD97-2120	G. *bulloides*	300-301	0.1988	0.0013	-801	1	12980	60	14417
124690	MD97-2120	mixed benthics	300-301	0.1412	0.0008	-859	1	15720	50	17865
120245	MD97-2120	N. *pachyderma*	300-301	0.1740	0.0016	-826	2	14050	80	16020
124691	MD97-2120	mixed benthics	310-311	0.1286	0.0008	-871	1	16475	50	18796
120247	MD97-2120	N. *pachyderma*	310-311	0.1397	0.0014	-860	1	15810	90	18657
120248	MD97-2120	N. *pachyderma*	330-331	0.1302	0.0016	-870	2	16380	110	19011
120249	MD97-2120	N. *pachyderma*	340-341	0.1252	0.0019	-875	2	16690	130	19306
120250	MD97-2120	N. *pachyderma*	344-345	0.1213	0.0017	-879	2	16950	120	19513
120251	MD97-2120	N. *pachyderma*	350-351	0.1205	0.0022	-880	2	17000	150	19540
120252	MD97-2120	N. *pachyderma*	355-256	0.1232	0.0014	-877	1	16820	100	19403
118039	MD97-2120	G.*b* & N.*p*	360-361	0.1205	0.0028	-879	3	17000	190	19636
118040	MD97-2120	G.*b* & N.*p*	370-371	0.1106	0.0033	-889	3	17690	240	20234
118041	MD97-2120	G.*b* & N.*p*	380-381	0.1149	0.0028	-885	3	17380	200	19635
118043	MD97-2120	G. *bulloides*	390-391	0.1027	0.0044	-897	4	18280	350	20930
118042	MD97-2120	N. *pachyderma*	390-391	0.1057	0.0027	-894	3	18050	210	20642
118044	MD97-2120	G. *bulloides*	417.5-418.5	0.0974	0.0039	-903	4	18710	330	21591

Table S2 Age model for MD97-2120

Depth (cm)	Age (kyr)	Sedimentation rate	Species	Age Control points	Reference
22.5	2058	10.93	G. *bulloides*	$\Delta^{14}C$	Pahnke et al. 2003*
36.5	3664	8.72	G. *bulloides*	$\Delta^{14}C$	Pahnke et al. 2003*
98.5	7869	14.74	G. *bulloides*	$\Delta^{14}C$	Pahnke et al. 2003*
212.5	13150	21.59	G. *bulloides*	$\delta^{18}O$	EPICA 2006
236.5	14750	15.00	G. *bulloides*	$\delta^{18}O$	EPICA 2006
282.5	16650	24.21	G. *bulloides*	$\delta^{18}O$	EPICA 2006
312.5	18150	20.00	G. *bulloides*	$\delta^{18}O$	EPICA 2006
330.5	19011	20.91	N. *pachyderma*	$\Delta^{14}C$	this study*
344.5	19513	27.89	N. *pachyderma*	$\Delta^{14}C$	this study*
390.5	20786	36.14	N. *pachy*+ G. *bull*†	$\Delta^{14}C$	this study*
418	21591	34.16	G. *bulloides*	$\Delta^{14}C$	this study*

* converted to calendar ages using Calib 5.0.1; ΔR=-160 ± 40, based on local modern reservoir ages[18]
† ^{14}C ages for both N. *pachyderma* and G. *bulloides* averaged for this stratigraphic pick.

Table S3 Age model for RR0503-JPC64

Depth (cm)	Age (kyr)	Sedimentation rate	Species	Age Control points	Reference
37	5590	6.62		Whatane tephra	Lowe et al., 2008
90	9505	13.28		Rotoma tephra	Lowe et al., 2008
90.5	13720	0.00		Waiohau tephra	Lowe et al., 2008
128.5	16350	14.07	G. *inflata*	$\delta^{18}O$	EPICA 2006
132.5	16651	13.29	G. *inflata*	$\Delta^{14}C$	this study*
138.5	16880	26.20	G. *inflata*	$\Delta^{14}C$	this study*
142.5	17122	16.53	G. *inflata*	$\Delta^{14}C$	this study*
153	17625	15.46		Rerewhakaaitu tephra	Lowe et al., 2008
164.5	18322	22.07	G. *inflata*	$\Delta^{14}C$	this study*
170.5	18846	11.45	G. *inflata*	$\Delta^{14}C$	this study*
190.5	19638	25.25	G. *inflata*	$\Delta^{14}C$	this study*

* converted to calendar ages using Calib 5.0.1; ΔR=-50 ± 50, based on local modern reservoir ages[18]

Table S4 alternate age models for RR0503-JPC64 and MD-2120

Core	Depth (cm)	Age (kyr)	Sedimentation rate	Species	Age Control points	Reference
JPC64	37	5590	6.62		Whatane tephra	Lowe et al., 2008
JPC64	90	9505	13.28		Rotoma tephra	Lowe et al., 2008
JPC64	90.5	13720	0.00		Waiohau tephra	Lowe et al., 2008
JPC64	123.5	16253	12.63	G. *inflata*	$\Delta^{14}C$	this study
JPC64	132.5	16651	22.61	G. *inflata*	$\Delta^{14}C$	this study
JPC64	138.5	16880	26.20	G. *inflata*	$\Delta^{14}C$	this study
JPC64	142.5	17122	16.53	G. *inflata*	$\Delta^{14}C$	this study
JPC64	153	17801	15.46		Rerewhakaaitu tephra	Lowe et al., 2008
JPC64	164.5	18322	22.07	G. *inflata*	$\Delta^{14}C$	this study
JPC64	170.5	18846	11.45	G. *inflata*	$\Delta^{14}C$	this study
JPC64	190.5	19638	25.25	G. *inflata*	$\Delta^{14}C$	this study
2120	22.5	2058	10.93	G. *bulloides*	$\Delta^{14}C$	Pahnke et al. 2003
2120	36.5	3664	8.72	G. *bulloides*	$\Delta^{14}C$	Pahnke et al. 2003
2120	98.5	7869	14.74	G. *bulloides*	$\Delta^{14}C$	Pahnke et al. 2003
2120	204.5	12050	25.35	G. *bulloides*	$\delta^{18}O$	EPICA 2006
2120	282.5	16650	16.96	G. *bulloides*	$\delta^{18}O$	EPICA 2006
2120	312.5	18150	20.00	G. *bulloides*	$\delta^{18}O$	EPICA 2006
2120	330.5	19011	20.91	N. *pachyderma*	$\Delta^{14}C$	this study
2120	344.5	19513	27.89	N. *pachyderma*	$\Delta^{14}C$	this study
2120	390.5	20786	36.14	N. *pachy*+ G. *bull*†	$\Delta^{14}C$	this study
2120	418	21591	34.16	G. *bulloides*	$\Delta^{14}C$	this study

* converted to calendar ages using Calib 5.0.1; using local modern reservoir ages[18]
† ^{14}C ages for both N. *pachyderma* and G. *bulloides* averaged for this stratigraphic pick